Optics Letters

Retrieving the coherent artifact in frequency-resolved optical gating

Esmerando Escoto,[1,*] Rana Jafari,[2] Rick Trebino,[2] and Günter Steinmeyer[1,3]

[1]Max Born Institute for Nonlinear Optics and Short Pulse Spectroscopy, Max-Born-Str. 2A, 12489 Berlin, Germany
[2]School of Physics, Georgia Institute of Technology, 837 State Street Northwest, Atlanta, Georgia 30332, USA
[3]Department of Physics, Humboldt University, Newtonstr. 15, 12489 Berlin, Germany
*Corresponding author: escoto@mbi-berlin.de

Received 1 May 2019; accepted 16 May 2019; posted 28 May 2019 (Doc. ID 366522); published 12 June 2019

When confronted with a pulse train whose intensity and/or phase versus time varies from pulse to pulse, multi-shot pulse-measurement techniques usually exhibit a coherent artifact (CA), which substantially complicates the interpretation of the measurement. In frequency-resolved optical gating (FROG), such instabilities are indicated by discrepancies between the measured and retrieved FROG traces. Here we consider the simultaneous retrieval of the CA and the average pulse characteristics from a single FROG trace in the limit of significant fluctuations. We use a modified generalized projections algorithm. Two electric fields are simultaneously retrieved, while the data constraint is updated as the algorithm progresses using only the assumption that the trace can be modeled as the sum of two spectrograms, one corresponding to the pulse and the other corresponding to the CA. An additional flat-spectral-phase constraint is added to one of the fields to ensure that it only reacts to the presence of the CA. Using this novel retrieval method, the complete retrieval of the characteristics of pulses in an unstable train from FROG traces is demonstrated.

https://doi.org/10.1364/OL.44.003142

The generation of ultrashort pulses nearly exclusively starts with mode-locked laser oscillators, which typically operate at megahertz repetition rates. The pulse energies of these primary sources are on the order of a nanojoule or less, corresponding to $<10^9$ photons in a single pulse. These photon numbers are prohibitively low for the use of single-shot characterization techniques, which can only be applied after subsequent amplification of the oscillator pulses. Therefore, the characterization of mode-locked oscillators often requires averaging over millions of pulses, and nearly all measurement techniques developed to date implicitly rely on the temporal stability of the pulse train; that is, it is assumed that all pulses in the train exhibit an identical pulse shape. However, when pulses vary from shot to shot, noise effects can obscure the desired measurement, usually with a narrow peak located at zero delay in autocorrelation or FROG measurements. This peak is known as the coherent artifact (CA). The CA has been a long-standing problem in ultrafast optics and has been a cause of confusion for decades [1–3]. While often considered a problem of mode-locked dye lasers, similar instabilities have been observed in mode-locked semiconductor lasers [4] and fiber lasers [5]. Some modern (mainly interferometric) ultrashort pulse-measurement techniques measure *only* the CA—the shortest repeating substructure of the pulse train—leading to erroneously short pulse durations and mode-locking capabilities of the laser source [6–8]. The standards for measuring ultrashort laser pulses outlined in Ref. [9] recommend that a technique must provide at least an indication that the pulses being measured are unstable. Frequency-resolved optical gating (FROG) provides this indication to the user by an apparent "nonconvergent" result after running its pulse-retrieval algorithm, with the retrieved trace or spectrogram having a large error, even in the absence of noise [6].

Measures have been taken to understand and obtain more useful data from multi-pulse measurements of unstable pulse trains. One method, using FROG, is to retrieve multiple states at once by modifying the algorithm [10]. However, it would be impractical to do this in cases where the trace is a combination of millions of pulses, which is the case when using lasers with megahertz repetition rates. A quantitative analysis of pulse train instability has also been explored with multiphoton intrapulse interference phase scan, where a new parameter called fidelity as a function of added chirp was defined [11]. This fidelity parameter can be used to determine if the source of instability is phase or amplitude noise and can also tell by how much the nonlinear conversion efficiency can be affected by the instability of the pulses [12].

It has been shown that second-harmonic generation (SHG) FROG with the generalized projections (GP) algorithm [13] retrieves the average pulse shape, even in the presence of significant pulse shape fluctuations; however, there is a tendency to underestimate the pulse length [6,8]. Although SHG FROG does not provide a "typical" pulse in the train, instead yielding a smoothed average pulse, other versions of FROG, such as polarization-gate and cross-FROG, provide good typical pulses [6,8]. As yet, however, no approach yields quantitative information about both the CA and the pulse simultaneously.

In this Letter, we present a way to retrieve the underlying pulse characteristics from SHG FROG traces in the presence of

instabilities. We modify the GP algorithm to be able to retrieve more information about the pulse train than has been demonstrated previously. Specifically, we isolate the traces due to the CA and the average pulse, and separately retrieve them from a single measured spectrogram. Both of these traces can be represented by single electric fields, simultaneously retrieved from a single FROG trace. For SHG FROG, the signal field for each pulse is represented by $E_{\mathrm{sig},j}(t,\tau) = E_j(t)E_j(t-\tau)$, where $E_j(t)$ is the complex-valued electric field envelope as a function of time t. The expression for the FROG trace averaged over several pulses can be written as

$$I_{\mathrm{FROG}}(\omega,\tau) \equiv \frac{1}{N}\sum_{j}^{N}\left|\int_{-\infty}^{+\infty} E_{\mathrm{sig},j}(t,\tau)\exp(-i\omega t)\mathrm{d}t\right|^2, \quad \textbf{(1)}$$

where N is the number of pulses averaged in the measurement. The GP algorithm works by implementing the two constraints that compose the total knowledge available from the measured FROG trace: the mathematical constraint corresponding to the nonlinear optical process involved and the data constraint, which corresponds to the fact that the measured trace is the spectrum of the signal field. Implementation of the data constraint occurs by replacing the magnitude of the signal field with that of the measured trace, while the mathematical constraint is implemented by minimizing an error functional [14]. These two constraints are repeated iteratively until the algorithm converges to the solution (a trace that matches the measured one).

At first sight, our new retrieval algorithm may appear reminiscent of blind FROG retrieval. The latter technique has also been termed twin recovery of electric-field envelopes by the use of FROG (TREEFROG), where each iteration alternates between optimizing one of two fields [15]. Another inversion algorithm, called the principal component GP algorithm (PCGPA), can retrieve two electric fields by using the concept of an inner product between the two different fields [16]. However, both TREEFROG and PCGPA cannot be applied as a solution to our problem, since the FROG traces in CA retrieval cannot mathematically be modeled as the result of a cross-correlation of two fields, but they rather appear as the sum of two separate FROG traces which can be written in the form

$$I_{\mathrm{FROG}}(\omega,\tau) = aI_{\mathrm{CA}}(\omega,\tau) + bI_{\mathrm{ave}}(\omega,\tau), \quad \textbf{(2)}$$

where I_{FROG}, I_{CA}, and I_{ave}, respectively, are the measured FROG trace, the FROG trace from the CA, and the FROG trace resulting from the random components of the pulse. The variables ω and τ represent the frequency and the delay. The coefficients a and b are real positive numbers that determine the relative intensity of the two traces. It has been rigorously proven for SHG autocorrelation that, in the limit of large pulse fluctuations, the corresponding values of a and b are equal [14,17]. In addition, in view of the fact that SHG FROG is a spectrally resolved autocorrelation, this implies that, for zero delay, the area of a vertical (zero-delay) slice of the SHG FROG trace is one-half base and one-half the CA. Finally, because the pulse trace and CA trace should have the same spectral widths, we can conclude that their heights should also be equal, so $a = b$ in SHG FROG in this limit. Of course, for less noisy pulse trains, the ratio is unknown and will likely depend on the specifics of the pulse train. The previous measurements of the CA indicate that a and b often have near identical values. Nevertheless, we left the choice of the ratio a/b to the algorithm.

A more recent technique used to solve the problem of retrieving two fields from one measurement is enabled by the time domain extended ptychographic iterative engine (tdePIE) [18,19]. The tdePIE works by updating both probe and gate pulse solutions on every iteration. This is done by using an update function which, interestingly, depends on the other field being retrieved. To create the algorithm used in this Letter, this concept is adapted for the GP algorithm, where both I_{CA} and I_{ave} are simultaneously retrieved from the measured trace I_{FROG}. An update function similar to Ref. [18] is formulated, with appropriate changes, because the signal being considered is a sum and is not a product as in the original formulation of the problem:

$$I_{\mathrm{CA}} = I'_{\mathrm{CA}} + \beta\left(\frac{I_{\mathrm{FROG}} - bI'_{\mathrm{ave}}}{a} - I'_{\mathrm{CA}}\right), \quad \textbf{(3)}$$

$$I_{\mathrm{ave}} = I'_{\mathrm{ave}} + \beta\left(\frac{I_{\mathrm{FROG}} - aI'_{\mathrm{CA}}}{b} - I'_{\mathrm{ave}}\right), \quad \textbf{(4)}$$

where β is the update rate, which controls the amount of change taken in each iteration and by how much the previous iterations influence the latest solution. The variables (ω,τ) are suppressed for brevity. In our implementation of the algorithm, we used $\beta = 0.01$, but the exact value of β was found to be rather uncritical for the success of the algorithm. However, a very large β may render the solution unstable and never convergent, while a very low one can cause stagnation of the algorithm. In the above equations, I' designates the retrieved trace from the previous iteration. Coefficients a and b are obtained by using simplex optimization in each iteration.

The update functions in Eqs. (3) and (4) are used before implementing the data constraint in the GP algorithm, where the signal amplitude is replaced by the measured one. In this case, instead of using the measured trace amplitude $\sqrt{I_{\mathrm{FROG}}}$, the two signal amplitudes are replaced by $\sqrt{I_{\mathrm{ave}}}$ and $\sqrt{I_{\mathrm{CA}}}$. The mathematical constraint remains the same, i.e., a distance function is minimized to determine the best-fitting fields, given the two signals in the time domain. An additional constraint is applied to one of the electric fields, forcing it to be a Fourier-transform-limited pulse with a flat phase, as this is the hallmark of a CA.

To test the algorithm, different sets of unstable pulse trains are generated using the same procedure as described in detail in Refs. [6,20], with two sets having identical widths with the sets used in Ref. [6]. Starting from a 1×4096 array with a temporal sampling rate of δt, a Gaussian field with a full width at half-maximum of $20\delta t$ corresponding to the stable component of the pulse is generated. The spectrum of this pulse can be obtained by using a discrete Fourier transform, which is then used to construct the unstable component of the pulse train. The spectra are centered at ω_0, with $\delta\omega$ representing the spectral sampling rate. A random phase is applied in the frequency domain. Then, after inverse-Fourier transforming to the time domain, the pulse is multiplied by a Gaussian envelope of variable temporal width. The resulting noise-like complex field is added to the stable component to create a single pulse. Each pulse train consists of 5,000 pulses constructed in this way. This method creates a pulse train, each with pulses that differ in both spectral and temporal domains, as can be seen in Fig. 1.

Three pulse trains are constructed with time envelopes of different widths: $59\delta t$, $126\delta t$, and $192\delta t$. The average FROG

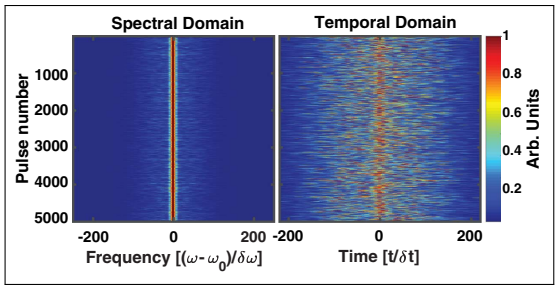

Fig. 1. Intensities of the pulses in spectral and temporal domains, for a time envelope with FWHM = $192\delta t$.

traces resulting from these are shown in Fig. 2, along with the FROG traces retrieved by using the algorithm. All retrievals resulted in low error values (G). Compared to directly using the unmodified GP algorithm as was done in Ref. [6], the new algorithm resulted in errors that are at least an order of magnitude lower. Moreover, additional information that can be obtained from the retrievals is the values of the coefficient a and coefficient b, which gives a valuable insight on how energy is distributed in the pulse train. The resulting values are consistent with the experimental measurements of the CA where the peak-to-background ratio is roughly 2 [21].

The retrieved electric field envelopes for I_{CA} are plotted in Fig. 3, corresponding to the retrieved traces shown in the rightmost column of Fig. 2. It can be seen that the shape of the CA is almost perfectly retrieved in all three attempts. As for the spectra, some small deviations are noticeable, which can be attributed to the narrow support of the pulse in the time domain, making it susceptible to noise in the spectral domain.

Figure 4 shows the retrieved electric field envelopes for the average pulse, corresponding to the retrieved traces in the third column of Fig. 2. All three reconstructed spectra correspond almost perfectly to the average spectrum, without the deviations present in Fig. 3(a). Note that the three spectra are overlapping; thus, only one is fully visible. In temporal domain, the reconstructed pulse shapes also fit well with the time envelopes used to construct the pulses. This is a significant improvement from using an unmodified standard retrieval algorithm, which would result in an underestimated pulse width, accompanied by a large G error indicating instability [6]. The RMS errors of the retrieved intensities, as compared to the average spectra and the time envelopes, are summarized in Table 1.

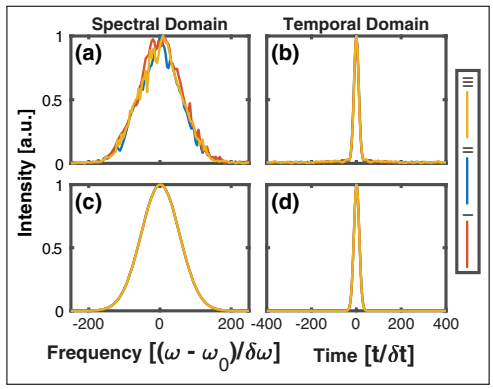

Fig. 3. Retrieved fields for I_{CA} in (a) spectral and (b) temporal domains. (c) and (d) Corresponding average spectrum and pulse shape for the stable component used in constructing the pulse trains. I: $59\delta t$, II: $126\delta t$, and III: $192\delta t$.

The algorithm will only be practical if it works without *a priori* knowledge, whether or not pulse instabilities are present, i.e., it must be able to determine on its own whether or not pulse instabilities are present. To test if the algorithm works in the absence of CA, a spectrogram made from a stable pulse train is fed into the algorithm, resulting in what is shown in Fig. 5. It can be seen that the algorithm still faithfully retrieves the correct trace, with essentially zero weight to I_{CA}, even though there is a considerable intensity in the middle part of the spectrogram similar to the earlier traces shown.

Several other sets of unstable pulses have been used to test the algorithm, where only the spectrum or only the temporal pulse shape varies, and the algorithm consistently converges to a lower error as compared to directly using GP. One problem that can be encountered, however, appears when the average spectrum is not simply the Fourier transform of the average temporal shape of the pulse. For example, this is the case when the temporal envelope is a double pulse, which requires a structured spectrum, while the average spectrum is smoothened due to fluctuations. In this case, the algorithm would converge to the closest electric field corresponding to the average spectrum and temporal shape of the pulse but, of course, would fail to achieve a good fit. Such situations present the limitation of our retrieval method.

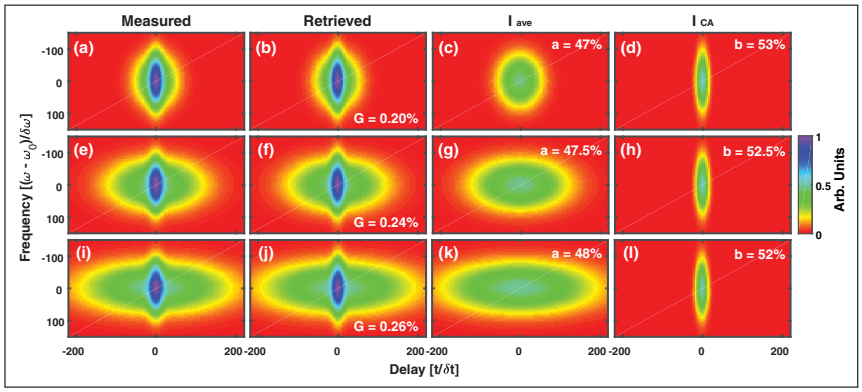

Fig. 2. Measured and retrieved FROG traces, along with the two traces corresponding to the CA and the average pulse. Top row, $59\delta t$; middle row, $126\delta t$; and bottom row, $192\delta t$. These can be directly compared with the results in Ref. [6].

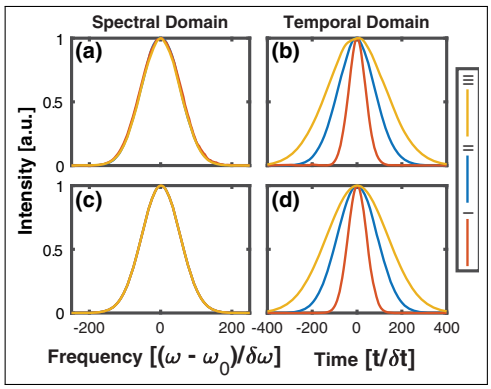

Fig. 4. Retrieved fields for I_{ave} in (a) spectral and (b) temporal domains. (c) and (d) Corresponding average spectrum and pulse shape for the unstable component used in constructing the pulse trains. I, $59\delta t$; II, $126\delta t$; and III, $192\delta t$.

Table 1. RMS Errors for the Retrieved Intensities in Spectral and Temporal Domains

	$59\delta t$		$126\delta t$		$192\delta t$	
	I_{CA}	I_{ave}	I_{CA}	I_{ave}	I_{CA}	I_{ave}
Spectral	3.3%	1.1%	3.2%	0.6%	3.6%	0.5%
Temporal	2.0%	2.1%	1.7%	2.7%	2.0%	1.8%

In cases when stable and unstable components share the identical average spectrum, the frequency marginal of the trace is unaffected. This means that the retrieval can be made more reliable by using the RANA approach [22], which provides a better initial guess for the algorithm, using information from the frequency marginal. Figure 6 shows the result of using the RANA approach. Note that all three pulse trains have the same average spectrum, so only one result is shown.

As a summary, the GP algorithm has been modified, using the concepts used in time domain ptychography, to simultaneously retrieve the CA and the average pulse characteristics of an unstable pulse train from a single FROG trace. The resulting algorithm retrieves two spectrograms which, when added together, correspond to the average FROG trace. The electric field envelopes corresponding to the two spectrograms represent the CA and the average pulse characteristics. Using our modified retrieval approach, standard SHG FROG measurements can

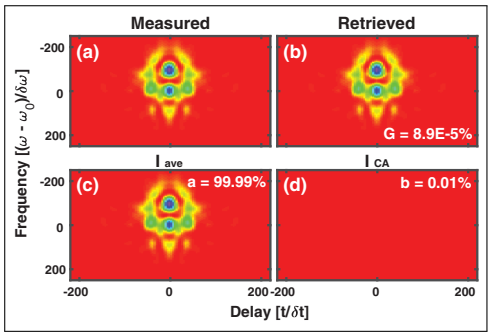

Fig. 5. Measured and retrieved FROG traces from a stable pulse train using the modified GP algorithm.

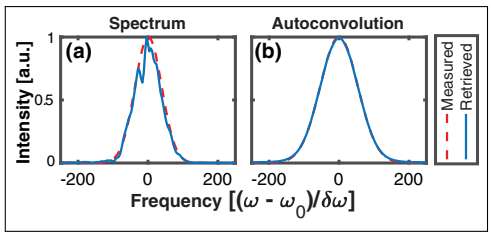

Fig. 6. Measured and retrieved spectra using the RANA approach, along with the autoconvolution coming from the frequency marginal of the trace with $192\delta t$.

be utilized to remove effects from the CA on the retrieved pulse shape and reliably recognize even scenarios of weak underlying instability. We believe that this approach opens up the possibility of studying the underlying structures of pulse trains when working with ultrashort pulses of uncertain stability.

Funding. Deutsche Forschungsgemeinschaft (DFG) (STE 762/11-1); National Science Foundation (NSF) (ECCS-1307817); Georgia Research Alliance (GRA).

Disclosures. Rick Trebino owns a company that sells pulse-measurement devices.

REFERENCES

1. M. A. Duguay, S. L. Shapiro, and P. M. Rentzepis, Phys. Rev. Lett. **19**, 1014 (1967).
2. J. A. Giordmaine, P. M. Rentzepis, S. L. Shapiro, and K. W. Wecht, Appl. Phys. Lett. **11**, 216 (1967).
3. Z. Vardeny and J. Tauc, Opt. Commun. **39**, 396 (1981).
4. K. G. Wilcox and A. C. Tropper, Laser Photonics Rev. **7**, 422 (2013).
5. A. F. J. Runge, C. Aguergaray, N. G. R. Broderick, and M. Erkintalo, Opt. Lett. **38**, 4327 (2013).
6. M. Rhodes, G. Steinmeyer, J. Ratner, and R. Trebino, Laser Photonics Rev. **7**, 557 (2013).
7. M. Rhodes, M. Mukhopadhyay, J. Birge, and R. Trebino, J. Opt. Soc. Am. B **32**, 1881 (2015).
8. M. Rhodes, Z. Guang, and R. Trebino, Appl. Sci. **7**, 40 (2017).
9. M. Rhodes, G. Steinmeyer, and R. Trebino, Appl. Opt. **53**, D1 (2014).
10. C. Bourassin-Bouchet and M. E. Couprie, Nat. Commun. **6**, 1 (2015).
11. V. V. Lozovoy, G. Rasskazov, D. Pestov, and M. Dantus, Opt. Express **23**, 12037 (2015).
12. G. Rasskazov, V. V. Lozovoy, and M. Dantus, Opt. Express **23**, 23597 (2015).
13. K. W. DeLong, D. N. Fittinghoff, R. Trebino, B. Kohler, and K. Wilson, Opt. Lett. **19**, 2152 (1994).
14. R. Trebino, *Frequency-Resolved Optical Gating: The Measurement of Ultrashort Laser Pulses* (Kluwer Academic, 2002).
15. K. W. DeLong, R. Trebino, and W. E. White, J. Opt. Soc. Am. B **12**, 2463 (1995).
16. D. J. Kane, G. Rodriguez, A. J. Taylor, and T. S. Clement, J. Opt. Soc. Am. B **14**, 935 (1997).
17. R. Trebino, E. K. Gustafson, and A. E. Siegman, J. Opt. Soc. Am. B **3**, 1295 (1986).
18. T. Witting, D. Greening, D. Walke, P. Matia-Hernando, T. Barillot, J. P. Marangos, and J. W. G. Tisch, Opt. Lett. **41**, 4218 (2016).
19. J. Hyyti, E. Escoto, G. Steinmeyer, and T. Witting, Opt. Lett. **42**, 2185 (2017).
20. T. Pfeifer, Y. Jiang, S. Düsterer, R. Moshammer, and J. Ullrich, Opt. Lett. **35**, 3441 (2010).
21. C. V. Shank and D. H. Auston, Phys. Rev. Lett. **34**, 479 (1975).
22. R. Jafari, T. Jones, and R. Trebino, Opt. Express **27**, 2112 (2019).